Tutora

Dra. Lourdes Mestres Vila
Departament de Química Inorgànica

Grau de Química

Treball Final de Grau

Synthesis and characterization of lead-free dielectric materials based on barium titanozirconate (BTZ)

Síntesis i caracterizació de materials dielèctrics lliures de plom basats en el titanozirconat de bari (BTZ)

Manel Mondelo Martell

June 2012

Universitat de Barcelona

I don't know anything, but I do know that everything is interesting

if you go into it deeply enough

Richard Feynmann

REPORT

CONTENTS

SUMMARY

The compound $Pb(Zr,Ti)O_3$, which presents a perovskite structure, is nowadays the material with most applications as a dielectric. Nevertheless, due to its high lead content, it is considered a hazardous material for the European Union, and therefore many efforts have been made in order to obtain materials with similar properties, but lead-free (and hence, environmentally friendly). Barium titanozirconate (BTZ) is studied with this aim, because of the high values of dielectric constant that it presents, especially near the temperature when the phase change from a tetragonal to a cubic structure occurs. Provided that both the maximum value for dielectric constant and the temperature at which the phase transition takes place depend deeply on the composition of the material, this essay presents the synthesis by the ceramic method of the compounds with general formula $BaTi_{1-x}Zr_xO_3$, being x=0.25, 0.30, 0.35, 0.40 and 0.45. This is made with the aim of finding the composition with an optimal electrical response that will allow its application in electronic devices.

The synthesis reaction is studied by Thermogravimetry (TG) and Differential Scanning Calorimetry (DSC). The temperature at which the decomposition and solid state reaction processes occur is found to be respectively 1033 ºC and near 1100 ºC. A phase change in barium carbonate is found at 880 ºC, and several endothermic peaks are found at higher temperatures.

The products obtained are characterized by Infrared Spectroscopy (IR), X-ray Diffraction (XRD), Scanning Electron Microscopy (SEM), Energy Dispersive X-ray Spectroscopy (EDS) and Impedance Spectroscopy (IS).

The IR study is made in order to find changes in the normal vibration modes of the compounds as the reaction advances. Middle-IR and far-IR analysis show the bands originated by the vibrations of the TiO_6 octahedrons.

The XRD analysis shows that the BTZ25 compound is obtained as a single-phased product after five thermal treatments, and has a cubic structure with a=6.033 Å. However, all the other compositions (BTZ30, BTZ35, BTZ40 and BTZ45) are found to present three different phases:

Barium titanate (BT), barium zirconate (BZ) and a heterogeneous solid solution of barium titanozirconate (BTZ).

Both BTZ25 and BTZ35 compounds are studied by SEM, with the aim of seeing the morphologic differences between a single-phased and a multiple-phased material. An homogeneous grain size distribution is found in BTZ25, while a grain size dispersion is found for the BTZ35 sample. EDS studies confirm a relation between the grain size and the Ti/Zr proportion.

IS allows the determination of the phase transition temperature of BTZ25, at 271K. The dielectric constant at this point presents a maximum at 5000, with a dielectric loss of 200.

RESUM

El compost $Pb(Zr,Ti)O_3$ (PZT), amb estructura tipus perovskita, és avui dia el material amb més aplicacions com a dielèctric. No obstant, pel seu contingut en plom és considerat un material perillós per la Unió Europea, i s'han fet molts esforços per a obtenir materials amb prestacions similars, però lliures de plom, per tal de substituir-lo. El titanozirconat de bari (BTZ) és un possible candidat, gràcies als elevats valors de constant dielèctrica que presenta, especialment a prop de la temperatura de transició de fase tetragonal a cúbica. Donat que tant els valors de permitivitat com la temperatura de la transició depenen profundament de la composició del material, en aquest treball es presenta la síntesi mitjançant el mètode ceràmic dels compostos amb fórmula general $BaTi_{1-x}Zr_xO_3$, amb x=0,25; 0,30; 0,35; 0,40 i 0,45; a partir de carbonat de bari, òxid de titani (IV) i òxid de zirconi (IV), amb intenció de trobar la composició amb una òptima resposta dielèctrica que permeti que el BTZ es pugui usar en dispositius electrònics.

La reacció de síntesi s'estudia mitjançant termogravimetria (TG) i calorimetria diferencial de rastreig (DSC), observant-se les temperatures a les que tenen lloc els processos de descomposició del $BaCO_3$ i la reacció en estat sòlid. Es troba un canvi de fase del carbonat de bari a 818 ºC, la temperatura de descomposició del mateix a 1033 ºC, i una sèrie de pics endotèrmics a temperatures més elevades.

Els productes obtinguts es caracteritzen per espectroscopia d'infraroig (IR), difracció de raigs X, microscopia electrònica de rasterig (SEM), espectroscopia d'absorció d'energia dispersada de raigs X(EDS) i espectroscopia d'impedàncies.

Es realitzen estudis d'espectroscopia d'infraroig per veure si es produeixen canvis en els modes normals de vibració dels compostos a mesura que avança la reacció. Els estudis en IR mitjà i llunyà mostren dues bandes degudes a modes normals de vibració de l'octaedre TiO_6.

L'estudi per difracció de raigs X mostra que el compost BTZ25 s'aconsegueix en forma de fase única amb els 5 tractaments tèrmics realitzats, amb una estructura cúbica amb a=6.033 Å. Per a la resta de composicions (BTZ30, BTZ35, BTZ40 i BTZ45) es troba la coexistencia de tres fases: titanat de bari (BT), zirconat de bari (ZT) i la solució sòlida de titanozirconat de bari (BZT).

Tant el compost BTZ25 com el BTZ35 s'estudien també per SEM per a veure les diferències morfològiques entre un compost amb fase única i un altre on tenim mescla de fases. S'observa una distribució homogenia de mida de grans en el BTZ25, i una dispersió important en les mides dels grans en el BTZ35. Els estudis per SEM-EDS en el BTZ35 confirmen una relació entre la mida dels grans i la proporció de Ti/Zr.

Mitjançant espectroscopia d'impedàncies es troba que el compost BTZ25 presenta una temperatura de transició de fase a 271 K. Per a aquesta temperatura la constant dielèctrica arriba a màxims de 5000 amb unes pèrdues dielètriques al voltant de 200.

INTRODUCTION

Solid inorganic compounds have been used and manufactured as materials by humans for thousands of years: from the flint used in the very first tools to the cement that we nowadays use for buildings, in addition to metals, alloys and glasses, technology has advanced at the same rate as our capability to improve our materials and take profit of this improvements.

Functional inorganic materials, in opposition with the structural materials, are those materials with applications that are not based in the crude mechanical strength or the external beauty, such as electronics, magnetism or optics[1]. These materials are often ceramics. The most simple of them, for instance, binary oxides of iron (for magnetic data storage), TiO_2 (for paints) or MoS_2 (a widely extended lubricant) have been used for a long time, but nowadays, especially since the discovery of the superconductor cuprates in 1987, much research is focused in new inorganic materials that show enhanced or even completely new properties with important potential applications as magnetic, optical or electronical materials[2]. These so called Advanced Ceramics or Materials, both in design and technologic terms, play now a fundamental role in the technology and the research: the studied systems have a greater complexity every day, for we are able to control more precisely the interatomic distances, the degree of covalency, the defects formation, the oxidation states of the elements and the microstructure of the material. All this makes it possible, therefore, to tailor our materials to obtain specific properties[2, 3].

One of the main applications of ceramics in contemporaneous world is in electronical devices such as sensors, actuators, transducers, capacitors... Dielectric materials are the basis for the manufacturing of these systems, and as the practical applications become of more critical importance, it has been necessary to develop new dielectrics able to answer the needs of these applications, through the control of both chemical parameters (composition, stoichiometry, homogeneity, purity…) and physical properties (morphology, particle size distribution, aggregates formation…)[3]. For instance, the development of electromechanical devices has been the main driving force for the development of new piezoelectric materials (*i.e.*

materials able to develop an electrical polarization proportional to an applied mechanical stress or viceversa), especially over the last 15 years[4].

In the area of capacitors and other devices that need high-permittivity dielectrics, perovskyte-type materials ABO_3 are the ones that have attracted more attention, for their excellent electrical properties derived from their structure. Of all the known dielectric materials, barium titanate ($BaTiO_3$) is the most largely studied, and is usually taken as the reference dielectric material[1, 3-8]. Its strong ferroelectrical properties were discovered in the 1940s in a British industrial laboratory, and a complete phenomenological theory of ferroelectricity was set out in 1949 by Devonshire[1].

Nevertheless, although being the reference material for ferroelectrics, barium titanate is not the most used material in electronic. Lead titanozirconate (PZT) has dominated the ferroelectric scenario since its discovery in the early 1950s, for this solid solution has large dielectric and piezoelectric properties in a composition near to a morphotropic phase boundary[4], which gives a great range of applications to this material. Moreover, a change in the ferroelectric *hard* and *soft* behaviour can be obtained with the addition of acceptor and donor dopants, respectively. However, a high amount of lead is necessary for the synthesis of this compound, which includes several cycles of calcination and milling that can release this metal to the environment. In addition, the recycling of the devices that contain PZT can be a hazard for humans and the environment. Because of this, and in spite of the excellent properties of lead titanozirconate, the European Union has included this material as a hazardous substance[9, 10]. Therefore, the efforts are now focused in the research for a new lead-free material with very similar properties to PZT, in order to replace the hazardous material with an environmentally friendly one.

Since the concepts discovered in barium titanate were the ones applied to PZT, a quite obvious option has been to take profit of the former to try to obtain a new lead-free material, with the properties of the later[11]. Substitution of Ti^{4+} by isovalent cations is a widely studied approach[8]. Zr^{4+} has been chosen to obtain a solid solution analogous to the PZT: the barium titanozirconate (BZT). This compound has a very high and broad dielectric constant, and its properties change drastically with the percentage of zirconium[12-15]. These facts give BTZ a great technological potential, and it has been established as one of the most important compositions for ceramic capacitors[11].

In this essay we will present the synthesis of barium titanozirconate by solid state reaction, with different proportion of zirconium. The process will be monitored doing X-ray diffraction

analysis, to check out whether the synthesis is correct or not. Then, the characterization of the material will be done to find out how the structure, morphology and electrical behavior change with the composition.

OBJECTIVES

The main objective of this essay is to find out the dependence of the electrical properties of barium titanozirconate with the proportion of Titanium and Zirconium. To achieve this purpose, the following points must be fulfilled:

- Obtain the compounds with the general formula $BaTi_{1-x}Zr_xO_3$ and x=0.25, 0.30, 0.35, 0.40 and 0.45 through the ceramic method, analyzing whether this method is or not a good synthetic approach.

- Study the reaction by thermal analysis (Thermal Gravimetry and Differential Scanning Calorimetry) and FT-IR.

- Find out the cell parameters and hence the unit's cell volume of the different compounds by X-ray diffraction. Relate this volume with the density of the material obtained.

- Characterize the compounds with different experimental techniques:

    o Study the morphology of the materials by Scanning Electron Microscopy.

    o Study the composition of the samples by Energy Dispersive Spectroscopy, focusing in the elemental distribution over heterogeneous phases.

    o Study of the electrical response of the material through Impedance Spectroscopy.

1. THEORY FUNDAMENTALS

The aim of this section is to introduce the theory necessary to understand the whole essay.

1.1 PEROVSKITE STRUCTURE

Perovskite is the name of the mineral $CaTiO_3$, but the particular lattice of this substance has given name to a whole family of cristalline materials with general formula ABO_3 that share the same structure. Perovskite oxides show electric and magnetic properties that make them so attractive. For this reason they have been studied extensively to develop new materials with improved properties.

The perovskite structure can be seen from the two perspectives:

a)   As a three-dimensional network of BO_6 octahedrons sharing corners, with the A cation in the central 12-coordinated position. This structure is showed in Figure 1.

b)   As a cubic close packed AO_3 array, with the B cations occupying ¼ of the octahedral holes.
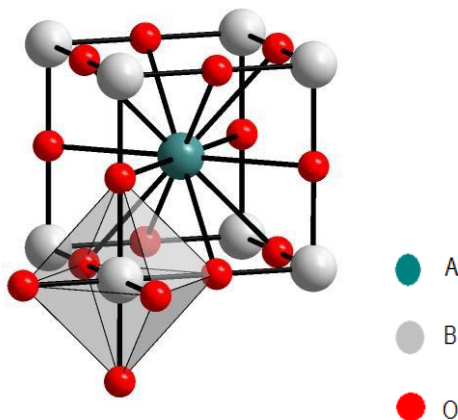

Figure 1: Unit cell for a ABO_3 perovskite structure.
Source: QES group, Universitat de Barcelona

There are many compounds with a structure based on a perovskyte lattice: titanates, tungstates, niobiates... However, most of them present distortions from the ideal cubic lattice,

such as tilted BO_6 octahedrons that may reduce the simetry of the structure and even change the coordination number of the central cation. These distortions give special properites to the specific material. For example, barium titanozirconate, which is the studied compound in this essay, presents a cubic perovskite lattice for low amounts of Zr, but with a higher proportion of zirconium it presents a tetragonal lattice and it becomes ferroelectric.

1.2 ELECTRICAL PROPERTIES OF DIELECTRIC MATERIALS

A dielectric material is an electric insulator. That means that in an electric field they do not transport charges in long-term, but remain polarized, as it happens with capacitors. Two main features define the usefulness of a dielectric material: dielectric strength and dielectric loss.

- Dielectric Strength, ε_r': A material's capability of supporting high voltages without undergoing a physicochemical change that turns it a conductor.
- Dielectric Loss, ε_r'': The amount of electrical energy that is lost, generally in form of heat, when an alternate current is applied to the material.

Dielectric materials do not transport charges when a voltage is applied on them, but their structure is polarized instead by the electric field. This polarization makes that a dielectric material in a capacitor increases the capacitance of the system, *i.e.* the system stores more charge for a given voltage. The relation between the capacitance of a vacuum capacitor, C_0, and the capacitance of a capacitor with a dielectric inside, C_1, gives the *relative permittivity* or *dielectric constant* of the material, ε_r':

$$\varepsilon_r' = \frac{C_1}{C_0}$$

This constant depends on the polarizability of the material. The macroscopic polarization for a pure dielectric material, in a linear approximation, is[6]:

$$P = \varepsilon_0 \chi_e E = \varepsilon_0 \varepsilon_r' E - \varepsilon_0 E$$

Where ε_0 is the free space permittivity and   is the dielectric susceptibility. This polarization has its origin in the sum of all the dipole moments p that the material has at microscopic scale:

$$p = \alpha E_{loc}$$

Here, α is the polarizability of the material and has five components[5,6]:

- Electronic polarizability (α_e): Caused by the displacement of the electron cloud in the atoms. It occurs in all solids, regardless of crystalline structure, temperature or AC frequency.

- Ionic polarizability (α_i): Appears due to the slight displacements of positive and negative ions in the crystalline lattice under an applied electric field. It appears in non-centrosymmetric space groups for ionic solids.

- Dipolar or orientation polarizability (α_d): It occurs when substances with a permanent electrical dipole are present. These dipoles are randomly oriented if there is no electric stimuli, but tend to align to an applied electrical field polarizing the material. This effect is temperature-dependent, as the thermal oscillations tend to perturb the dipoles' alignment.

- Space charge polarizability (α_s): It is found in materials with some sort of long-range migration phenomenon that causes an inhomogeneity in the charge distribution throughout the material.

- Domain wall polarization (α_w): Decisive in ferroelectric materials, which present electrical domains. The domains with a favorable orientation with respect to the applied electric field tend to grow in expenses of the other domains.

If an AC is applied, the different contributions will be more or less important: low frequencies will allow the atoms, ions dipoles and the whole solid to reorganize and contribute to the global polarizability, but as frequency increases (10^9 Hz), only the more rapid processes will contribute to the polarization: electronic and ionic polarization (Figure 2). In a good dielectric material, these should be the most important contributions to polarizability.
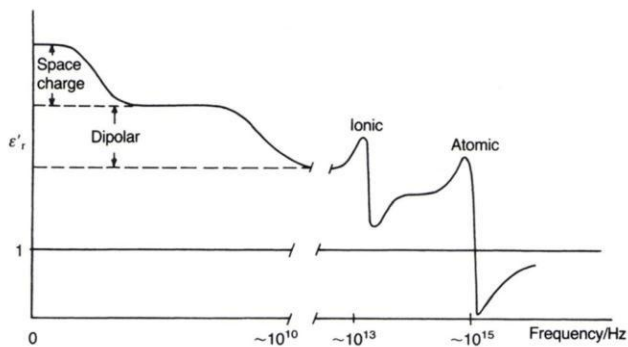

Figure 2: Different contributions to ε_r depending on the frequency. Source: ref [5].

BaTiO$_3$ is a ferroelectric material at room temperature. In the tetragonal phase, the TiO$_6$ octahedrons are deformed and lose the inversion centre, with the Ti^{4+} displaced from it. This distortion gives a spontaneous polarization of the material. The polar axis may be different for different grains, and that will create electrical domains, that is, areas of the solid with a different orientation of the dipolar moment, as showed in Figure 3.
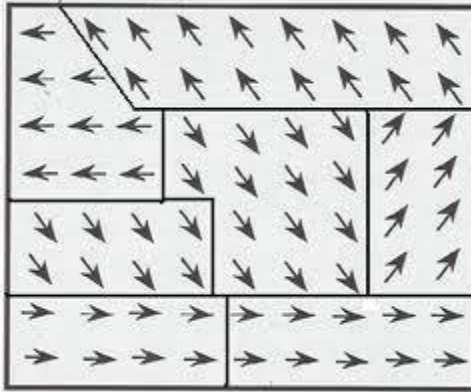

Figure3: Example of domains in a solid. Arrows point to the same direction as the dipolar moment.

This effect disappears in cubic BaTiO$_3$, which is the stable phase at high temperatures. This is because a cubic centrosymmetric group has an inversion center, and any polar vector would have another with the same norm and direction but opposite sense; therefore the structure would be non-polar. However, the addition of Zr to the system decreases the phase transition temperature, and for x>0.12 the cubic structure will be stable at room temperature and the substance will be a pure dielectric material. Hence, our BZT compounds should show a dielectric behavior but without ferroelectricity, since the polarization will not remain when the external electric field disappears.

1.3 THE SOLID STATE REACTION

For a chemical reaction between two species to occur (does not matter if atoms, ions or molecules) they have to encounter themselves in the same point of the space at the same time, which requires a high mobility of the reactants. This is the kind of chemical procedure found in gaseous or liquid phase (either if the reaction is between melted reactants or we are working in a dissolution), but in solid state the mobility of the particles is very low at room temperature, almost inexistent. Therefore, to produce a reaction between substances in the solid state it is

vital to improve the mobility of the particles in the solid, allowing the diffusion of the components to create a new substance.

The ceramic method was the first and most obvious approach to sintetize a solid from solid precursors: it is based on heating a mixture of precursors (usually oxides, carbonates…) to high temperatures, in order to enhance the diffusion of the substances[5]. If the mixture is homogeneus and the reactant phases are in close contact, the diffusion will take place through the grain boundaries, and the new desired phase will be formed as seen in Figure 4.
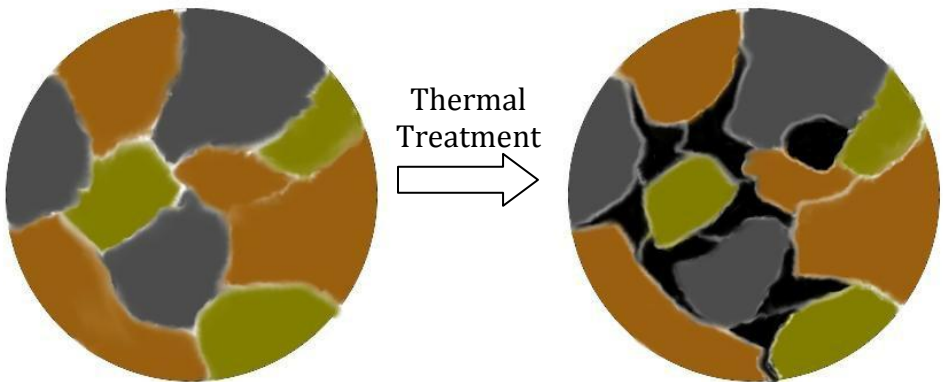

Figure 4: Scheme for a typical solid-state reaction. Grey, brown and yellow phases are the reactants; black phase represents the reaction product.

However, as the new phase grows in the grain boundaries the formation of the product will become more difficult, because that phase will not allow the contact between the reactants, and therefore the particles will need to pass through the product phase in order to react. In the long run, this may avoid completely the formation of product[5]. To prevent this to happen, it is necessary to grind the solid and homogenize it by mixing the powder[3]. This procedure (called *grinding*) will produce *fresh* interfaces between the reactant phases, and a dispersion of the product phase, allowing again the solid state reaction. Repeated cycles of thermal treatment and grinding will finally produce a single phase product.

1.4 CHARACTERIZATION TECHNIQUES

1.4.1 Thermal analysis

A calorimetric technique is based in the interaction of the sample with heat. This interaction can give us information about chemical and physical processes such as reaction, morphotropic phase changes or physical state changes, and about the intrinsic thermodynamic properties of these processes. In this essay two of these techniques will be used: Termogravimetry (TG) and Differential Scanning Calorimetry (DSC).

TG studies the variation of the sample's mass with the temperature. This gives information about the exact temperature where a process involving a mass change in the sample occurs. Typically, the processes studied are desolvatation, desorption, and decomposition of solids. When the weight of the sample is represented in front of the temperature, a characteristic curve is obtained. The temperature of the process can be studied from the midpoint of this curve, and find out if the decomposition is complete by comparing the weight loss observed in the experiment with the theoretical weight loss.

On the other hand, in DSC experiments our sample and a reference (which must be a substance that must not suffer any kind of transformation within the temperature ranges in which the experiment is carried out) are heated at the same time, and the difference in heat needed to maintain our sample at the same temperature that the reference is measured. When the temperature at which a physicochemical process occurs is reached, the sample will absorb heat without increasing temperature (endothermic process), or will release it spontaneously, increasing the temperature (exothermic process). Plotting the increment of heat needed to maintain the two substances at the same temperature, a graph with peaks and valleys is obtained. These peaks and valleys represent the endothermic and exothermic processes the sample passes through. An example of a TG and DSC plot is shown in Figure 5.

Both experiments were carried out in a *SDT Q600* instrument provided by the DIOPMA group, from the Department of Material's Science and Metallurgic Engineering (Universitat de Barcelona).
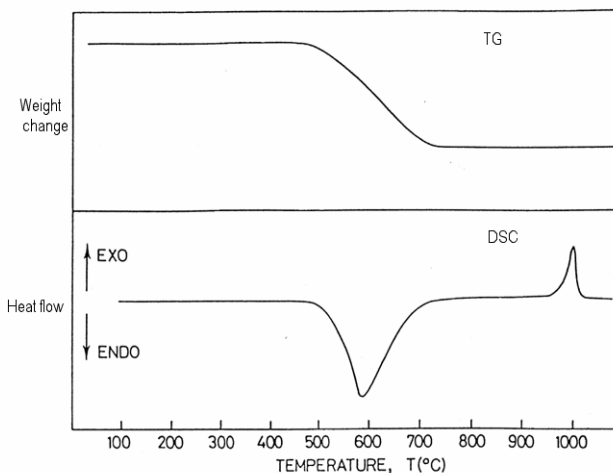
Figure 5: Example of a TG and DSC plot. Source: Ref [5]

1.4.2 Infrared Spectroscopy

Infrared spectroscopy is a useful tool for structural determination. The information can be found by the study of the normal vibration modes of the species in the crystal: IR radiation has the precise wavelength necessary to excite the vibrational states, so the absorption of radiation in this range can be related with the symmetry and structure of the compounds.

Following the harmonic oscillator model for molecular vibrations, it can be found that the approximate wavelength necessary to excite a quantum vibrational mode from state 0 to 1 is given by[16]:

$$\tilde{\nu} = \frac{1}{2\pi c}\sqrt{\frac{k}{\mu}}$$

Hence, the wavelength of the absorbed radiation depends on the mass of the atoms and the strength of the bonding. In our case, the most interesting vibration is the band due to the stretching of the M-O bond in the MO_6 octahedron (with M=Ti or Zr)[17]. The vibrations of TiO_6 and ZrO_6 will be significantly different, because the mass and the force constant of the M-O bond are different for Zr and Ti. Nevertheless, if the sample is a single phase, the spectrum will show an average of the spectra of the $BaTiO_3$ and $BaZrO_3$, since the structure itself would be a

combination of these compounds. Hence, an IR spectrum should show whether there is or not a single phase before the sample is studied by X-Ray diffraction.

The middle IR study was made with *Thermo Nicolet Avatar 300 FT-IR*. The far IR study was made with a *Bomem D3D FTIR* spectrometer from the CCiTUB.

1.4.3 X-Ray Diffraction

The term *diffraction* includes different processes that occur when a wave encounters an obstacle or slit of a characteristic length of the order of the wavelength of the wave. For instance, a linear wave *bends* when an obstacle is placed in its path, or when it has to pass through a small slit.

A very studied and well-known diffraction phenomenon is the diffraction of a wave by a diffraction lattice. In 1820 Fraunhofer discovered that, when a light beam passed through a glass in which an ordered pattern of several lines had been carved very close one to another (the Diffraction Lattice), the radiation passing through this ordered structure showed an interference pattern due to the diffraction of the beam. X-ray crystallography is based in this phenomenon.

On the early 20th century no evidence existed of the periodic structure of crystals but this hypothesis, which appeared after the observation of the regular faces and structures of some minerals, was widely accepted. The discovery of the X-rays in 1895 by W.C. Röntgen and the determination of its approximate wavelength by Wien, Walter and Pohl between 1908 and 1912 was an inflexion point in the knowledge of crystals: in 1912, Max Von Laue obtained a diffraction pattern exposing a single crystal of $CuSO_4$ to a beam of X-rays, demonstrating the periodic structure of crystals and giving birth to a new and powerful characterization technique: the X-ray diffraction.

X-ray diffraction is based in the scattering of the X-ray beam by the periodic structure of the crystal, which is to be seen as a conjunction of crystallographic planes acting as a diffraction lattice. When the beam passes through a sample it is diffracted by the different planes in many directions. The interference of the diffracted waves gives a pattern of maximums and minimums, called diffraction pattern.

Once the diffraction of X-rays by crystals was achieved, and therefore the crystalline structure of solids demonstrated, W.H. Bragg and W. L. Bragg discovered that a constructive

interference was produced in the same way as if there was a reflexion on a plane mirror. This diffraction follows the so called Bragg's Law:

As it can be seen in Figure 6, for a given wavelength λ and distance between planes d, constructive interference will only occur if the incidence angle θ makes the additional distance the beam travels to arrive to the second plane to be a multiple of the wavelength, so the reflected waves are in phase. Otherwise, the waves will be out of phase and the interference will be destructive.
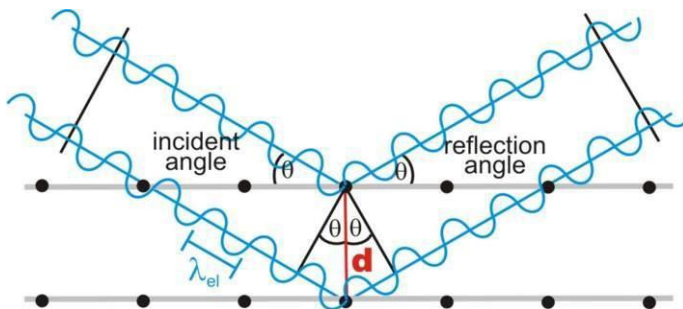

Figure 6: Representation of the Bragg's law. Here, the reflected waves are in phase.
Source: Swiss Federal Institute of Technology Zurich (www.microscopy.ethz.ch)

There are different methodologies to obtain a diffraction pattern, but they can be classified in two main categories: monocrystal XRD and powder XRD[18]. In powder XRD, which is the technique that will be used in this essay, the sample is a polycrystalline powder. This type of sample is formed by thousands of micrometric crystals randomly oriented, and statistically there will be always some crystals that form the right angle with the X-rays beam to produce a reflexion according to Bragg's Law. Hence, irradiating a polycrystalline sample a characteristic diffraction pattern, unique for each substance, is obtained. Although this technique does not give as much information as monocrystal XRD, and some reflections may not be observed, it allows the determination of the most of the crystallographic planes by comparing the diffraction pattern of a sample with the reference of JCPDS-ICDD[1] cards. Once the crystallographic planes are found, the crystallographic parameters of the unit cell (a,b,c, α, β and γ) can be found.

XRD studies were carried out with a *PANalyticalX'Pert PRO MDP* diffractometer, with a Ge (111) monochromator. The radiation used was the Kα line of Cu at 40kV and 30mA, and the diffraction pattern was registered for 2θ angles from 10° to 80°, with a scanning speed of

---

[1] Join Committee for Powder Diffraction Standards-International Centre for Diffraction data.

1°/min. The diffraction patterns were studied with the *X'Pert HighScore50* software.

1.4.4 Scanning Electron Microscopy

The interaction of electrons with matter in general, and solids in particular, is a complex subject of study in which many processes are involved: absorptions, emissions, reflections, transmissions… These processes are summarized in Figure 7, where the drop-like areas in which the different processes occur can be seen too; each one has a characteristic penetration power in the sample. The great amount of phenomena means that a lot of information can be obtained by irradiating the sample with electrons, and that is the reason why many techniques for solid characterization are based in electron-solid interactions. Electronic microscopy is one of these techniques.
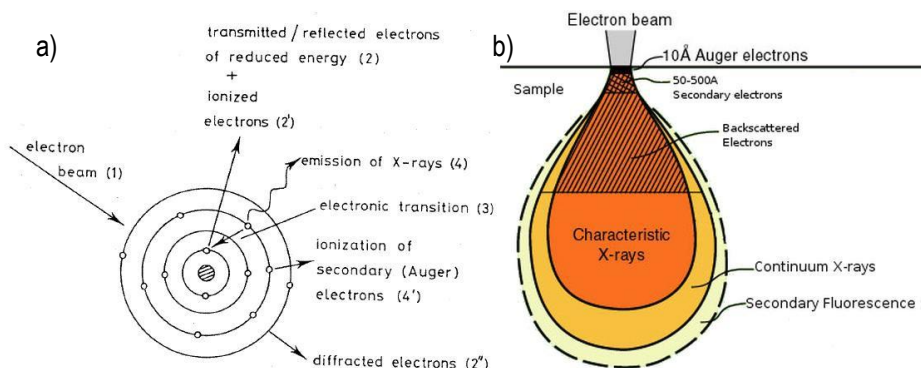

Figure 7: a) Electronic processes that give the signals for electronic microscopy; b) Interaction volume of a electron beam with a solid sample. Different processes occur at different depths and hence give different information. Source: Ref [5] & Northern Arizona University (www4.nau.edu/microanalysis/Microprobe)

The maximum resolution of an optical microscope (*i.e.*, the minimum distance *d* two points must be separated in order to be seen as two different points) is limited by the wavelength of visible radiation, as it was postulated by E. Abbe:

$$d = \frac{0.61\,\lambda}{n \cdot \sin\alpha}$$

Hence, diminishing the wavelength of the radiation used it would be possible to achieve better resolution. Instead of using more energetic electromagnetic radiation, short wavelengths are achieved by using accelerated electrons, for which the relation between the momentum and the wavelength is given by the de Broglie equation:

$$\lambda = \frac{h}{p} = \frac{h}{mv}$$

It is usual to work with the accelerating voltage instead of momentum, yields:

$$\lambda = \frac{h}{\sqrt{2meV}}$$

The electrons used for microscopy are usually emitted by a tungsten filament or a LaB_6 crystal, with an accelerating voltage of 50 to 100 kV, giving a resolution that achieves 2 Å in the most powerful High-Resolution Electron microscopes, allowing the direct observation of the crystal lattice.

There are two main techniques within electron microscopy: Transmission Electron Microscopy (TEM) and Scanning Electron Microscopy (SEM). In TEM the electrons that pass through the sample without changing their energy are detected; the intensity of the beam in every point of the sample gives information about the thickness and the density of that point. This technique has intrinsically better resolution than SEM, but it needs a special pre-treatment to make the sample thin enough.

In SEM, which is the technique that will be used during this characterization, the electron beam is focused in a small spot (50 to 100 Å in diameter). Two kinds of electrons can then be detected: the Backscattered Electrons (BSE) and the Secondary Electrons (SE). BSE are the electrons that are scattered after an elastic collision with the atoms in the surface of the material. The scattering depends on the weight of the atoms the electrons collide with: heavy atoms scatter electrons more strongly than light atoms, so the contrast of the image can be related with the atoms present in each zone of the solid. Unfortunately, since these electrons are scattered by atoms that are found quite deep in the solid, so a three-dimensional image of the solid's surface is not obtained. In contrast, SE are the electrons emitted by the sample when it is bombed with electrons. These electrons are emitted in all directions by atoms that can be at distances of 0.5 micrometers from the surface. Since the electrons detected have low energy, they are easily deviated from its trajectory, and therefore a three dimensional image of the material is obtained. This image can be used to extract information about the surface's morphology, even about single particle's size and shape.

Although SEM has in general less resolution than TEM (from 1 to 0.1 µm), it needs no special pre-treatment of the sample, except the deposition of a thin metallic or graphite layer to prevent the ionization of the sample, provided it is non-conductive.

The study of the solid's surface by SEM was made with a *JEOL JSM-480* microscope, coupled with a *Stereoscan 260 EDS analyser* (see below) present in the CCiTUB.

1.4.5 Energy Dispersive X-ray Spectroscopy

The interaction of electrons with a solid sample gives another interesting phenomenon: when a sample is bombarded with high energy electrons, the atoms present in the solid are ionized emitting electrons from all their electronic shells, including their core-shells. When an electron from the valence shell decays to relax the system it emits X-ray radiation of a precise wavelength (corresponding to the energy gap between the two shells). These X-rays are characteristic of the element, so scanning the X-rays emitted by the sample the elements present in it can be found out.

EDS is especially useful when coupled with an electronic microscope, since it is possible to focus in the small portion of the sample that is being observed through the microscope (such as a single particle of phase) and analyse at the same time its composition. Other operating mode is to scan the whole sample detecting just one element, and then make a mapping of the concentration of the element throughout the solid.

1.4.6 Impedance Spectroscopy

Impedance Spectroscopy is an excellent tool for studying the electrical response of dielectric materials, because it allows the separation of the different contributions to the total polaritzability of the material, and therefore to the dielectric constant[19].

This technique is based in the application of an AC to a pellet made of the material that is going to be studied placed between two electrodes (usually, a thin film of gold on two opposite sides of the pellet). This system is to be seen as a circuit such as the one seen in Figure 9.
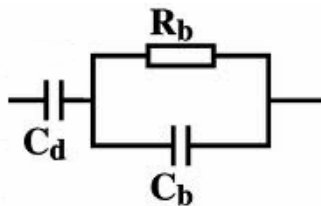

Figure 8: Equivalent circuit for a dielectric material. The resistance R_b represents the resistance the material offers to the current (high in a dielectric), and the two capacitors C_d and C_b the capacitance of the electrodes and that of the bulk ceramic respectively.

Hence, it is possible to relate the dielectric constant with the capacitance of this circuit:

$$C = \frac{\varepsilon_r \cdot A}{d}$$

But since this is an AC system, the capacitance of the material is a complex value with two contributions:

$$\varepsilon_r^* = \varepsilon_r' - j\varepsilon_r''$$

Where the real part is the dielectric constant, while the imaginary one represents the dielectric loses in form of heat.

As any imaginary number, the complex permittivity can be represented in polar coordinates (figure 10). In this case, the phase lag "δ" between Voltage and Intensity is the angle of the vector that represents the permittivity. As the frequency increases, δ changes from 90° to a minimum (depending on the material), reducing the dielectric constant and increasing the dielectric loses.
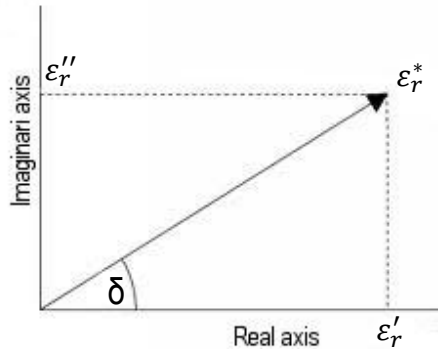

Figure 9: Polar representation of complex permittivity.

For this study, the intensity passing through our sample for known voltage and frequency will be measured, and system's impedance Z^* (*i.e.* the opposition that the material offers to the pass of current throughout it) will be found. This impedance is an imaginary magnitude, and it is related to V and I through:

$$Z^* = \frac{V}{I}$$

Then, impedance is related to the complex permittivity:

$$\varepsilon_r^* = \frac{1}{Z^* \cdot j \cdot C_0}$$

And the two components of the complex permittivity are then separated knowing the phase lag between V and I, which is related with the AC frequency.

The measures were carried out in a *Precision LCR Meter* (Agilent E4980A) provided by the CEMAT group, from the Applied Physics Department (UPC).

2 EXPERIMENTAL PROCEDURE

Five different compositions of barium titanozirconate with a general formula $BaTi_{1-x}Zr_xO_3$ have been prepared, ranging between a 25 and a 50 per cent of the titanium being substituted by zirconium with steps of 5% between the different compositions. These compounds will be referred to as BTZ100X from now on. The raw materials used during this synthesis have been $BaCO_3$ (Sigma-Aldrich 99%), TiO_2 anatasa, (Sigma-Aldrich 99%) and ZrO_2 (Riedel-de Haën/Sigma-Aldrich 99%).

The synthesis of these compounds was carried out through the ceramic method. This is a solid state synthesis method that consists in heating a mixture of precursors (usually oxides, carbonates…) to high temperatures, in order to obtain the desired product by the diffusion of the atoms in the crystalline lattice.

First of all, the titanium and zirconium oxides were treated in a muffle furnace at 900ºC during 8 hours, with the aim of dehydrate and decarbonize them, while barium carbonate was heated at 220ºC during 24 hours to remove any trace of water. Then, an accurate mixture of the reactants (±0.1mg of precision for every reactant) was made to obtain 6g of the final product (BTZ100X). To weight the reactants with high precision is of critical importance, since in a quantitative solid state reaction like this, which will lead to a solid solution, the stoichiometry will be exactly that derived from the reactants mixture. The mixture was then pulverized and homogenized in an agate mortar to ensure the contact of grains with different composition at micrometric scale. Once homogenized, the mixture was turned into pellets of 1g to increase the contact between the different grains, applying a pressure of ≈450 MPa.

The BTZ25 and BTZ30 compositions underwent the same cycle of thermal treatment/grinding, which is schematized in Figure 11. First of all, a thermal treatment at 1250°C was made, to decompose the barium carbonate and begin to form the $BaTi_{1-x}Zr_xO_3$ phase (the temperature was chosen with the aid of a thermogravimetry of the reactants' mixture)**.** Then, the pellets were quenched (*i.e*, cooled fast, with a high temperature gradient) in air, and then grinded and pelletized again. The grinding and re-pelletizing ensures, as it has been said before, the homogenous distribution of the grains with different compositions, enhancing the effectiveness of the diffusion process. After this process, the pellets were heated at 1500°C to continue with the solid state reaction.

Finally, the pellets were grinded and pelletized again in order to apply a third thermal treatment at 1500°C. This third thermal treatment is the *sintering* process, and has the aim of increasing the density of the pellets, because a high density is critical for the electrical characterization of the compounds. In this step the cooling was not fast, but with a rate of 2°C/min. This was done to avoid the possibility of crack formation due to the high thermal stress that the material would experience in a quenching process.
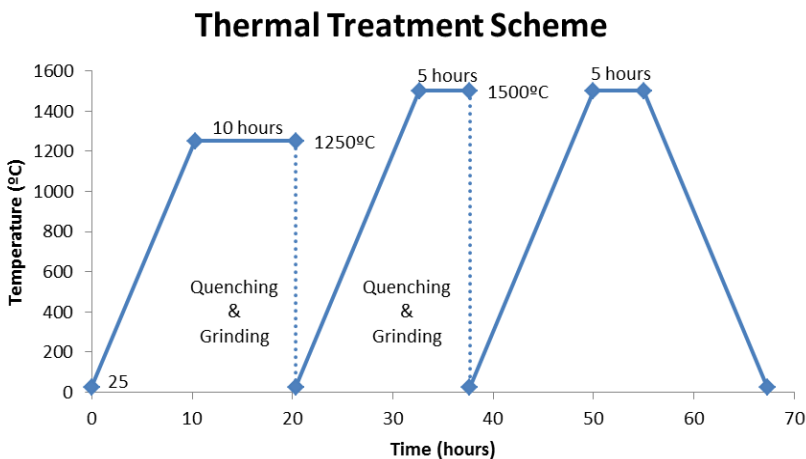

Figure 10: Thermal treatment scheme for the BTZ25 and BTZ30 pellets.

The compounds BTZ25 and BTZ30 underwent this cycle. Once sintered, the pellets showed a heterogeneous aspect: the pellets with a 25% of zirconium (BTZ25) had blue and light-yellow areas, while the other compositions were light yellow but with brown stains. The X-ray characterization of the powders (Figure 12) demonstrated the existence of 3 different phases, as

it can be seen in Figure 12: there are three maximums in each diffraction peak, that according to the JCPDS-ICDD cards correspond to the $BaZrO_3$ (BZ), the $BaTi_{1-x}Zr_xO_3$ (BTZ) and the $BaTiO_3$ (BT) phases (00-003-0632, 00-036-0019 and 00-003-0726 ID number, respectively).
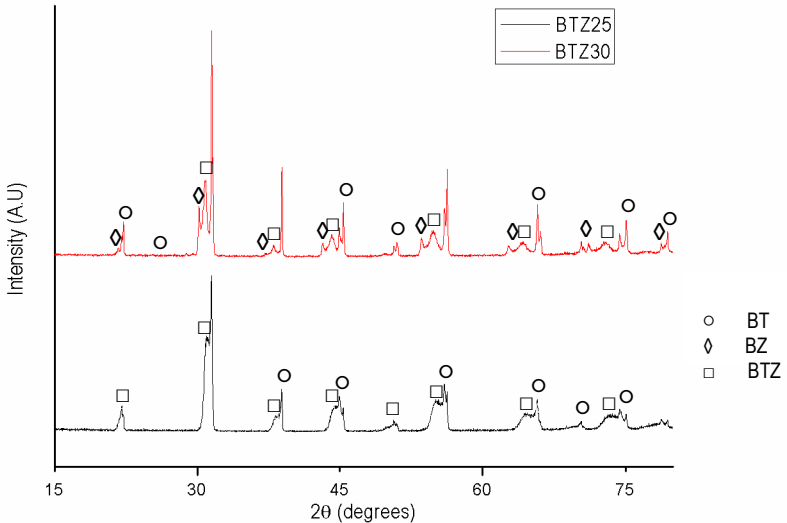

Figure 11: Diffraction pattern for the sample BTZ25 and BTZ30 after 3 thermal treatments. The different phases are pointed.

These results forced us to redesign our synthesis scheme, and a 4th thermal treatment was added to the process, heating up to 1500° during 5 hours more. Once the thermal treatment was completed, BTZ25 pellets had a homogeneous aspect, with a color between light blue and grey, whether the other compositions had a homogeneous light yellow color.

All the 5 compositions were again studied by X-ray diffraction. The diffraction patterns in Figure 13 show that BTZ25 is now a single phased material, while the other four compositions are still a mixture of barium titanate, barium zirconate and barium titanozirconate, although the amount of solid solution phase has increased (as it can be seen by the highness of the central diffraction peak).
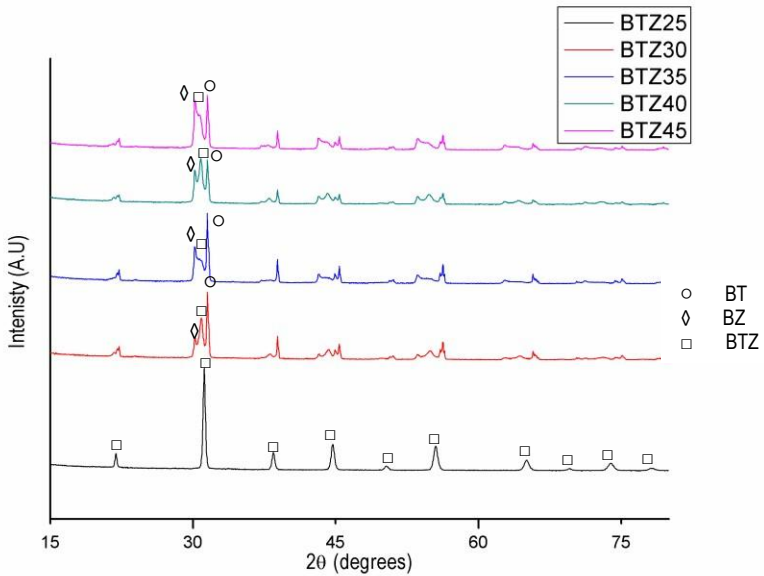
Figure 12: Diffraction patterns for the BTZ25, BTZ30, BTZ35, BTZ40 and BTZ45 after 4 thermal treatments. The peaks corresponding to the different phases are pointed in the most intense signals.

These results motivated the addition of another thermal treatment in order to try to get single-phased products in all compositions. While BTZ25 was prepared for its characterization, since it was the only single phased product, the other compositions were grinded, and they were heated again at 1500ºC, but this time for 10 hours (Figure 14).

At the same time, a new synthetic scheme was carried out: inspired by the synthetic process that appears in the JCPDS-ICDD card for the $BaTi_{0.75}Zr_{0.25}O_3$, a mixture of reactants prepared to obtain the compound BTZ45 underwent a first thermal treatment at 1250ºC for 10 hours in order to decompose de barium carbonate and start the solid state reaction, and a second thermal treatment (after the grinding of the pellets) at 1500ºC for 48 hours that was supposed to be enough to produce the solid state reaction and allow the diffusion of the cations in the crystalline lattice to obtain the solid solution.
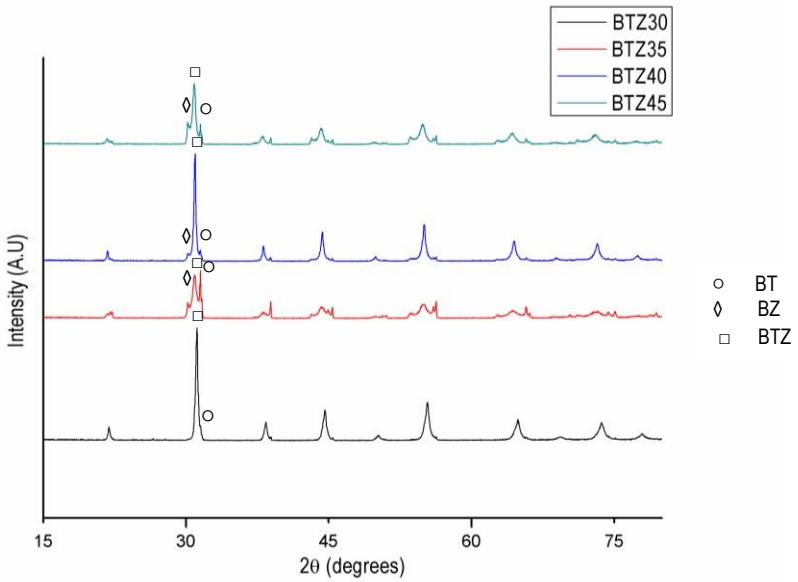
Figure 13: Diffraction patterns for BTZ30, BTZ35, BTZ40 and BTZ45 after five thermal treatments.

The X-ray diffraction analysis of the samples showed that there was not a single phase product yet in any of the compositions. What is more, in case of the BTZ45 sample that had experienced just two thermal treatments, there is almost no $BaTi_{0.55}Zr_{0.45}O_3$, as it can be seen in Figure 15. This shows the importance that the grinding has in a solid state synthesis process.
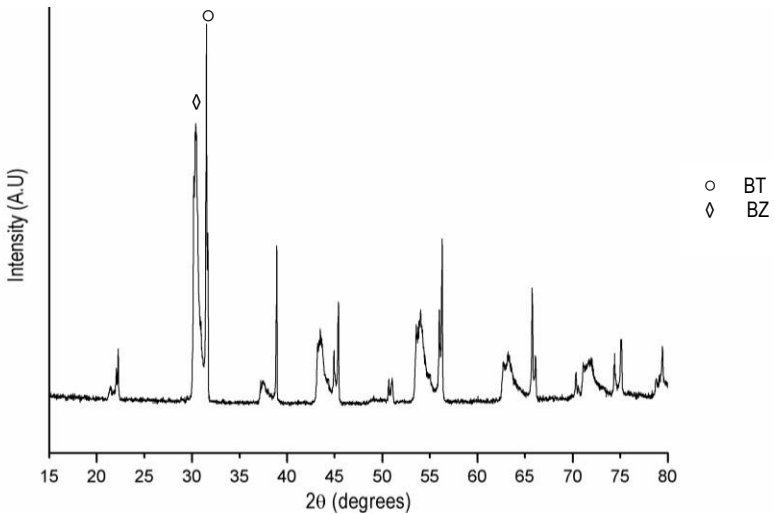

Figure 14: Diffraction pattern for the BTZ45 sample with 2 long thermal treatments.

Probably a sixth thermal treatment would have produced the single phase products, but it could not be completed due to deadline.

This synthesis method is very slow and expensive for all the energy needed to heat the furnace from room temperature each time a thermal treatment is done. In order to improve the process and make it more efficient, the duration of the thermal treatments must be optimized. We have seen with BTZ45 that very long thermal treatments are not useful, because if we do not grind the sample we avoid a correct diffusion of the elements to give the solid solution. On the other hand, a single thermal treatment of 10 hours has improved a lot the formation of the solid solution (as it can be seen in Figure 15). Hence, 10 hours may be a better time for the thermal treatments and would allow the formation of the materials with less time and energy.

3. CHARACTERIZATION

3.1 THERMAL ANALYSIS

A sample of the reactant mixture for BTZ25 was studied by Thermal Gravimetry and Differential Scanning Calorimetry. The results are shown in Figures 16 and 17.

For the thermogravimetry, a weight decrease for the sample is observed. The percentage of loose is coherent with the change expected for the complete decomposition of $BaCO_3$, taking into account the experimental error: a 15.23 % less of the total weight for the sample, for the theoretical loss of 15.8 %.

However, the mechanism of the decomposition of the carbonate in the reactant mixture seems to be more complex than it would be if the barium carbonate was pure. According to ref. 20, the mechanism for the formation of $BaTiO_3$ would be:

$$2BaCO_3 + TiO_2 \rightarrow Ba_2TiO_4 + CO_2$$

$$Ba_2TiO_4 + TiO_2 \rightarrow 2\ BaTiO_3$$
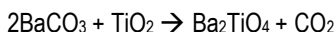
So it would be expected that a similar mechanism was followed for the formation of $BaZrO_3$.
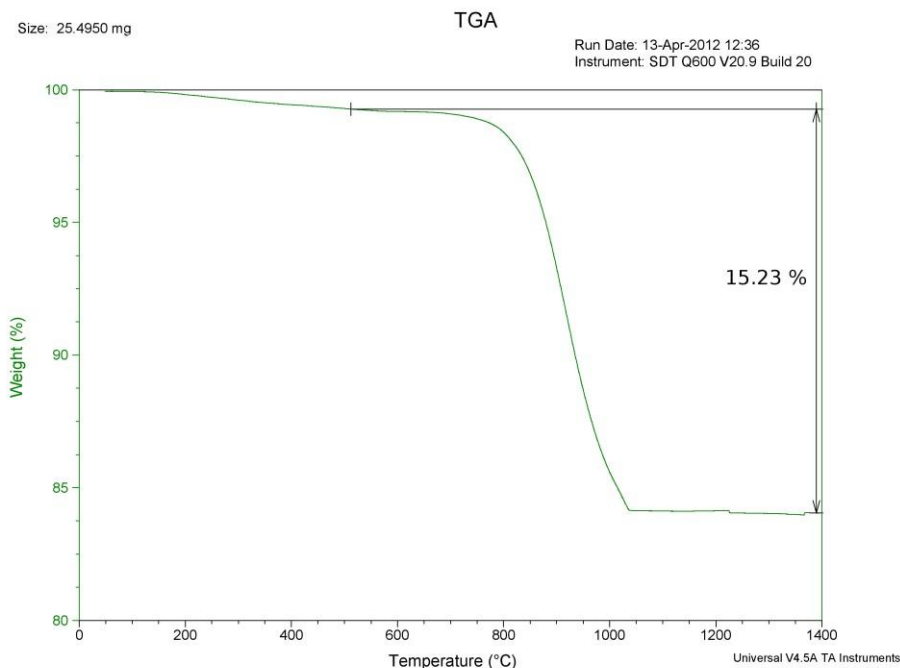
Figure15: Thermogravimetry scheme of the reactant mixture for BTZ25.

The results for the Differential Scanning Calorimetry shows the exact temperature were physicochemical processes occur. Four peaks can be seen in the experimental plot: the first one, at 818 ºC, corresponds to a polymorphic transformation from orthorhombic $BaCO_3$ to hexagonal form[20]. It is followed by a broad peak, which may be related with the polymorphic change from hexagonal to cubic phase of $BaCO_3$[20]. The fourth peak, at 1033ºC, is originated by the decomposition of $BaCO_3$ in the first steps of the reaction. Perhaps a large peak should be observed at T<1150 ºC due to the solid state reaction process, but the instrument gives no valid results beyond this point.
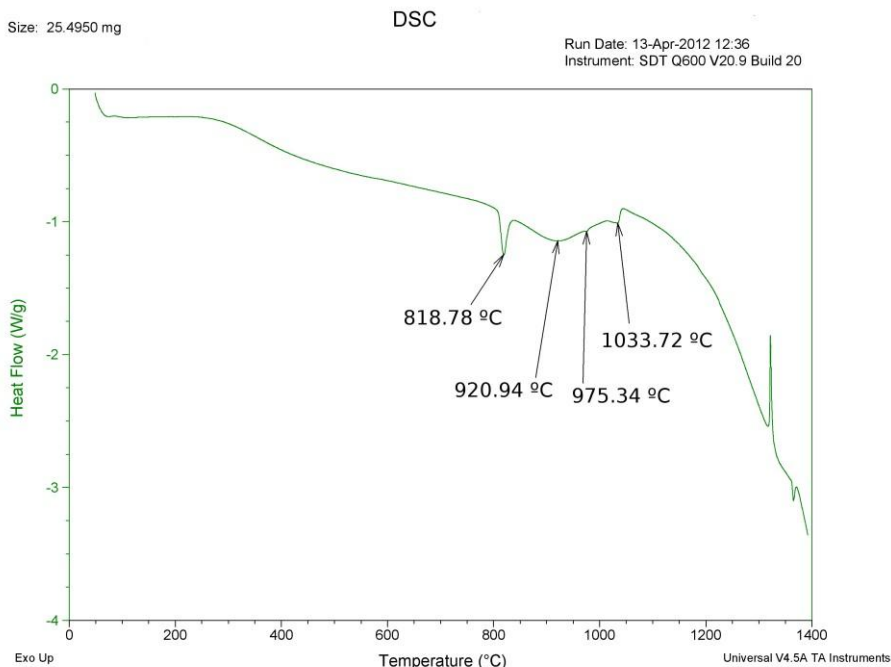
Figure 16: DSC plot for the reactant mixture of the sample BTZ25.

No peaks for polymorphic transformation of the titanium and zirconium oxides are found, although they should have appeared in the range of 400-500 ºC[21, 22].

3.2 INFRA-RED SPECTROSCOPY

The BTZ25 system was studied by IR spectroscopy from the reactant mixture to the third thermal treatment. Middle IR spectra are shown in Figure 17.

For the reactant mixture, the IR spectrum shows a peak 1400 cm^{-1}. This peak is the one from the C=O group in the carbonate anion. This band is much reduced when the sample undergoes the first thermal treatment, and completely disappears with the second thermal treatment (which is exactly equal to the third thermal treatment spectrum).
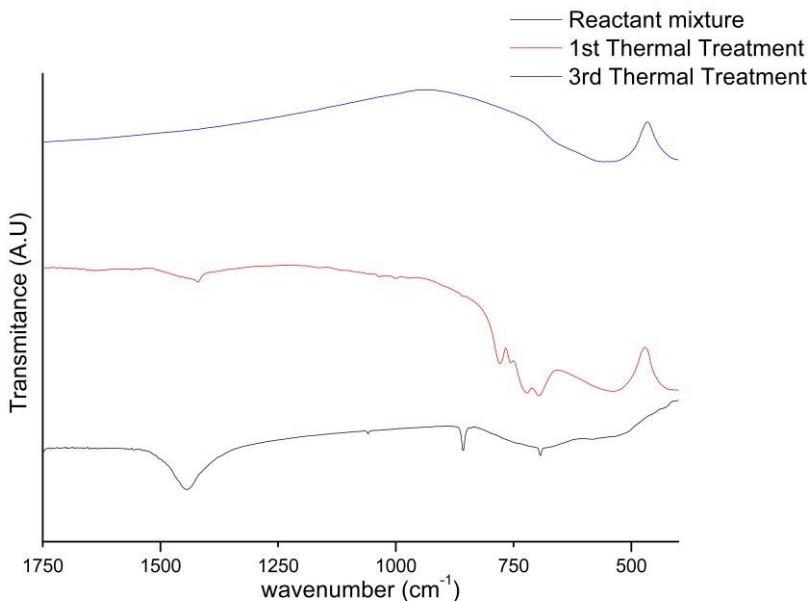
Figure 17: FT-IR spectra for the BTZ25 composition, with different thermal treatments.

The bands appearing between 650 and 850 cm^{-1} in the first thermal treatment spectrum, might be caused for some kind of intermediate phase produced during the solid state reaction, as it was told in section 3.1, since they disappear with subsequent thermal treatments.

For the third thermal treatment, in the lower wavenumber region at 500-400 cm^{-1}, two intense bands are found, the second band being truncated in the middle-IR spectrum. These two bands appear more clearly as the solid state reaction occurs, so they must correspond to normal vibrations of the BaTi$_{1-x}$Zr$_x$O$_3$ system. The infrared studies for barium titanate[17] assign the absorption bands to the normal vibrations of the TiO$_6$ octahedrons. It can be seen that the TiO$_6$ bands appear at low frequencies. Since Zr is heavier than Ti, the bands corresponding to the ZrO$_6$ system were expected to be found at too low frequencies to be studied by middle-IR spectroscopy. This motivated the study of the compound BTZ25 by far-IR spectroscopy, in order to observe these bands. The study was made in a range between 450 and 200 cm^{-1}, with polyethylene matrix (polyethylene has a low absorption in this range). The spectrum showed the same behavior in the range of 450-400 cm^{-1} that showed in the middle IR spectrum, but

instead of showing clear absorption bands related to the vibration of the TiO_6 and ZrO_6 octahedrons just a broad absorption band between 400 and 200 cm^{-1} appeared. This may be caused by the overlap of the bands corresponding to the vibrations of the two MO_6 systems.

3.3 X-RAY DIFFRACTION

Here the results for the XRD are shown for a single-phased product (BTZ25). The diffraction pattern for a multiple phased product (BTZ30) is also discussed.

3.3.1 Multiple-Phase products

Figure 18 shows the diffraction patterns for the BTZ30 compound after three, four and five thermal treatments. The general pattern of our diffraction diagram is coherent with the pattern for a perovskite structure, but it can be seen that each original diffraction peak is divided in three. Moreover, some of the peaks that appear at higher angles in every *triplet* are themselves double peaks. The only way to explain this is that more than one phase in our sample is obtained. Not considering the presence of impurities or secondary phases, the three phases present in the sample should be $BaTiO_3$, $BaTi_{1-x}Zr_xO_3$ and $BaZrO_3$. The different peaks arise because each phase present in a material will reflect the X-rays in a slightly different angle. To identify which peak corresponds to each phase it is necessary to recall Bragg's Law. Doing simple algebra:

$$\sin\theta = \frac{n\lambda}{2d}$$

Hence, a lower angle 2θ means a higher distance d between the crystallographic planes. This separation is closely related with the size of the atoms in the plane: the bigger their radius, the larger the interplanar distance, and therefore, the smaller the angles for which Bragg's Law is followed.

With this information, and knowing that the zirconium(IV) cation is bigger than the titanium(IV) one, it can be seen that the maximums that appear at lower angles in each group of three correspond to the $BaZrO_3$ phase, while the maximums appearing at the higher angles are due to the $BaTiO_3$ phase. Finally, the broad maximum appears because of the formation of the solid solution $BaTi_{1-x}Zr_xO_3$. The broadness of this signal means a low crystallinity of this phase, which arises from the fact that the $BaTi_{0.75}Zr_{0.25}O_3$ phase is not formed directly, but there is a

solid solution $BaTi_{1-x}Zr_xO_3$ with different x values throughout the sample. This means that there will be several compositions in this heterogeneous phase, and therefore different distances *d* between crystallographic planes. Since each distance will reflect X-rays in a certain angle, the resulting peak is broad and not narrow, as it is expected for a homogeneous phase.
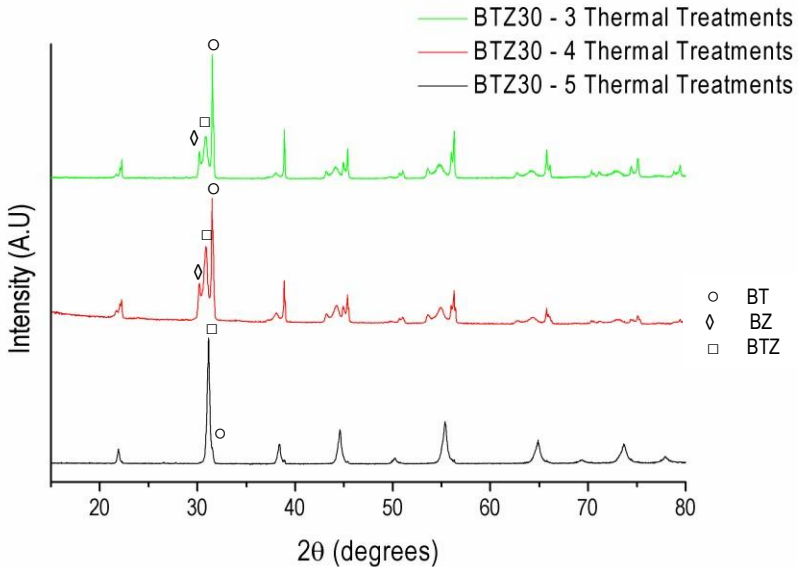

Figure 18: Experimental diffraction pattern for BTZ30 after 3, 4 and 5 thermal treatments.

But how can the double peaks for the signals assigned to barium titanate be exaplained? The answer lies in the stable structure of this compound at room temperature: as it was told in section 1.1, $BaTiO_3$ has a tetragonal lattice at room temperature, not cubic as the BTZ solid solution and barium zirconate. A tetragonal lattice gives a diffraction pattern very similar to the one of a cubic lattice, but without the same systematic extinctions, and hence some more peaks are seen for this phase. The stick pattern for the diffraction planes of a tetragonal lattice is shown in Figure 19.
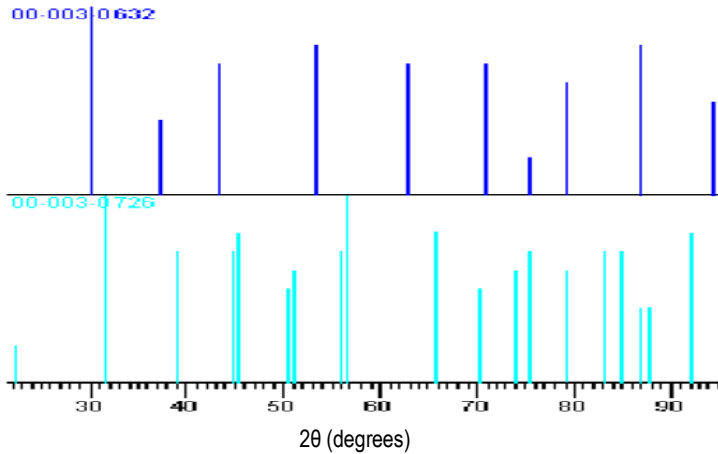
Figure 19: Stick pattern for the diffraction for cubic barium zirconate (up) and tetragonal barium titanate (down).

The number and position of the peaks gives information about the general structure of the sample, but their intensity also can be related to the relative amount of each phase. This is because if a great amount of a phase is present in our material, X-rays will be majorly scattered by this phase, and therefore the diffraction maximum corresponding to that phase will be larger than the ones coming from the other minor phases. That agrees with the relative size of the maximums present in each peak: since there is more titanium than zirconium the maximum due to $BaTiO_3$ is always more intense than the one due to $BaZrO_3$, and this difference is grater in BTZ30 than in BTZ45. On the other hand, the relative intensity of the solid solution phase changes, because it depends on how much product has been formed during the solid state reaction. In Figure 18 a growth and sharpening of the solid solution's peak with every thermal treatment can be observed, as the solid state reaction advances and the solution is formed.

Although the product is not a single phase, there are no peaks apart from the ones discussed above. This means that our sample does not contain any secondary phase or impurity.

3.3.2 Single-Phase products (BTZ25)

The only composition that has yielded a single phased material is BTZ25. Its diffraction pattern is shown in Figure 20.

Comparing with the JCPDS-ICDD card for $BaTi_{0.75}Zr_{0.25}O_3$ (00-036-0019), it can be seen that there is no secondary phase in the material, because all peaks in the experimental pattern can be assigned to a peak in the reference. Once this is stated, the next step is to relate each diffraction peak with a crystallographic plane. This is done again by comparing with the JCPDS-ICDD card, but a later refinement is needed to assure the correct assignation. This is done with the program AFFMA[23], which will fit the assignation with the demanded structure (cubic in our case) and tell whether the assignation is correct or not. The assignation of the BTZ25 sample is shown in the diagram in Figure 21.
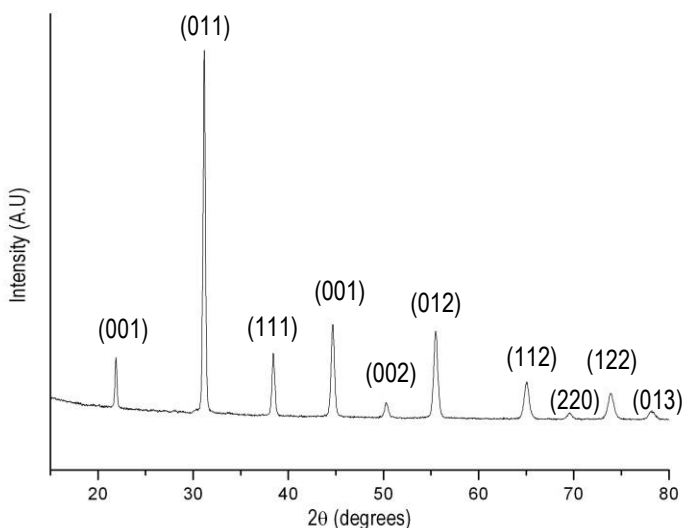

Figure 20: Experimental diffraction pattern for the compound BTZ25. Cristallographic planes assigned.

The program also computes the cell parameters for the material, giving the following result:

a=4.054(1) Å³   α=90°

b=4.054(1) Å³   β=90°

c=4.054(1) Å³   γ=90°

This provides a unit cell volume of:

$$V = a \cdot b \cdot c = 4.0543^3 = 66.61 \text{ Å}^3$$

As it was expected, this value lies between the volume of the unit cell of $BaTiO_3$ (64.41 Å³) and $BaZrO_3$ (72.83 Å³).

This volume is related with the maximum density expected for the material through:

$$\rho = \frac{M \cdot Z}{N_A \cdot V} = 6.08 \ g/cm^3$$

where

M=mass
Z=number of formulas per unit cell
N_A=Avogadro's number
V= Unit cell's volume

After the four thermal treatments the experimental density of the BTZ25 pellets was determined, by measuring and weighting them. Their density, relative to the expected density of 6.08 g/cm³, was 60 %; too low for a good study of the electrical response of the material.

Two additional thermal treatments at 1550 ºC were made in order to sinter the material. The final relative density achieved was 76.5 %. Although it was a low density, it was enough to allow a correct electrical characterization.

3.4 SCANNING ELECTRON MICROSCOPY - EDS

Fragments of the BTZ25 and BTZ35 pellets (four thermal treatments each) were covered with a thin film of gold through a *sputtering* Physical Vapor Deposition, and were studied with a Scanning Electron Microscope. The results are here explained.

3.4.1: Mutiple-Phase products

In Figure 21 the Secondary Electron micrographies for the BTZ35 pellet are showed. It can be seen that the sample has a high dispersion in grain size (from 5 to 1 micrometers), and the morphology is coherent with a low density material, with large spaces between grains. This may be due to the presence of three different phases in the pellet.
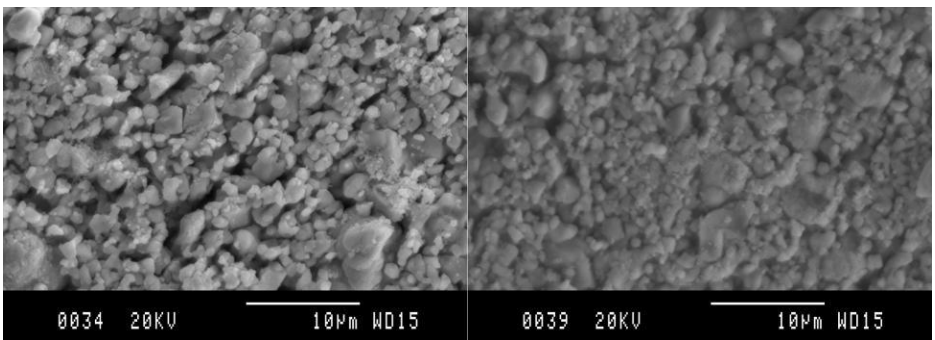

Figure 21: SEM-SE micrographs for the BTZ35 pellet at 3000X.

The mapping of titanium and zirconium throughout a portion of the material can be seen in Figure 22: in a) the micrography of the studied area is shown, while in b) and c) the concentration of Ti and Zr respectively is represented, with the lighter areas meaning a higher concentration of the element.
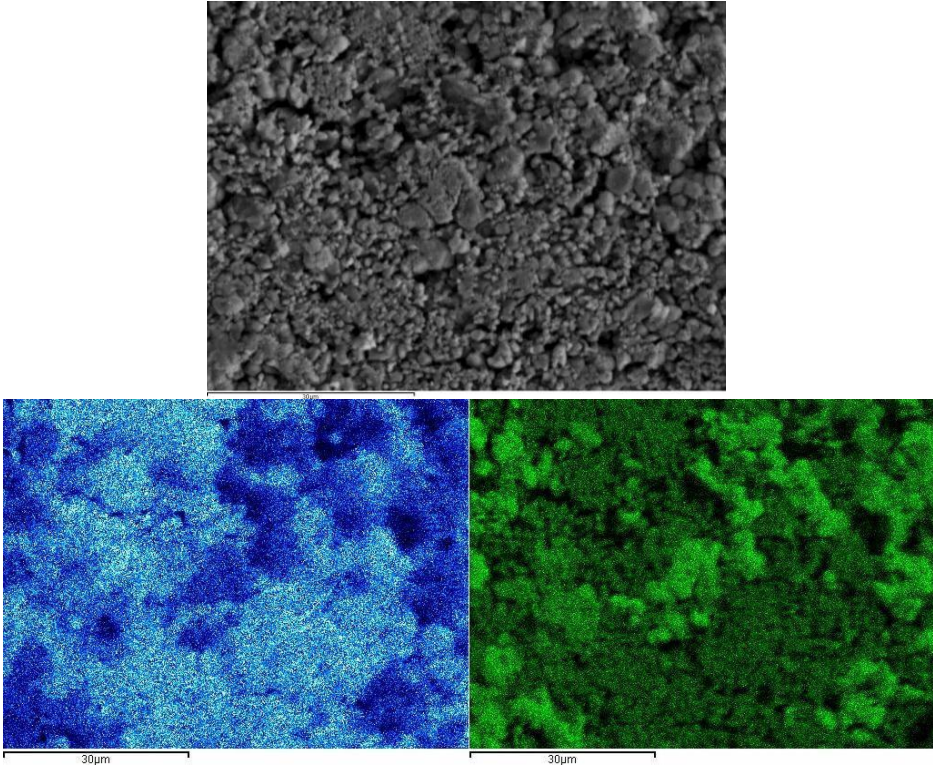

Figure 22: Micrograph of a BTZ35 pellet fragment. The Ti mapping is green, the Zr mapping is blue.

A perfect complementariness between images b) and c) exists: the lighter areas in one are the darker in the other. Moreover, the complementariness appears between the three pictures: the cracks can be seen in all them, and the greater grains seen in a) correspond mainly to areas with high concentration of zirconium, while the phase with a smaller grains size is that where there is more titanium. Hence, a relationship between the grain size and the percentage of zirconium in the solid solution could be established. The elemental distribution was confirmed by the analysis of two small portions of the sample by EDS, shown in Table 1.

Entry	Element	Atomic %	
		Ti-rich area	**Zr-rich area**
1	Ba	19.4	18.7
2	Ti	18.2	5.2
3	Zr	2.1	15.6
4	O	60.2	60.4

Table 1: Atomic percentage of Ti and Zr in two areas of the BTZ35 sample.

3.4.2: Single-Phase products

The SEM-SE micrographies for the BTZ25 pellet with 4 thermal treatments are shown in Figure 23.
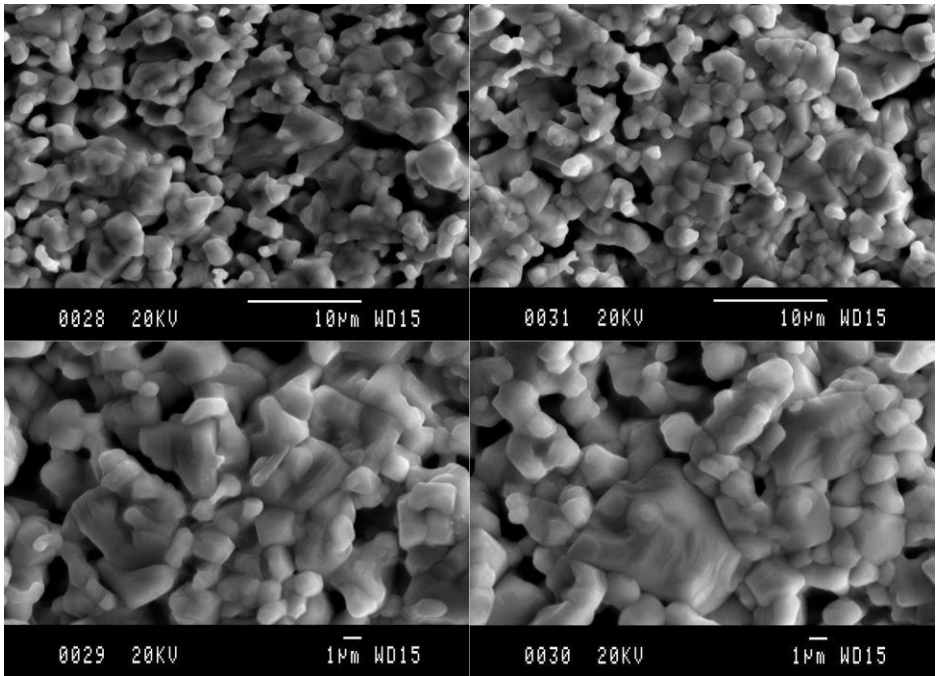

Figure 23: BTZ25 micrographs. Top: 3000X. Bottom: 5000X

Again, the porous aspect of the sample agrees with the measured density. Now the grain size is more homogeneous, although in certain areas of the pellet it seems to decrease or increase in comparison with others. A Ti and Zr mapping was done in order to find out if there is a compositional heterogeneity in the origin of this grain size change. The mapping showed in Figure 24 demonstrates no heterogeneity in the sample's composition.
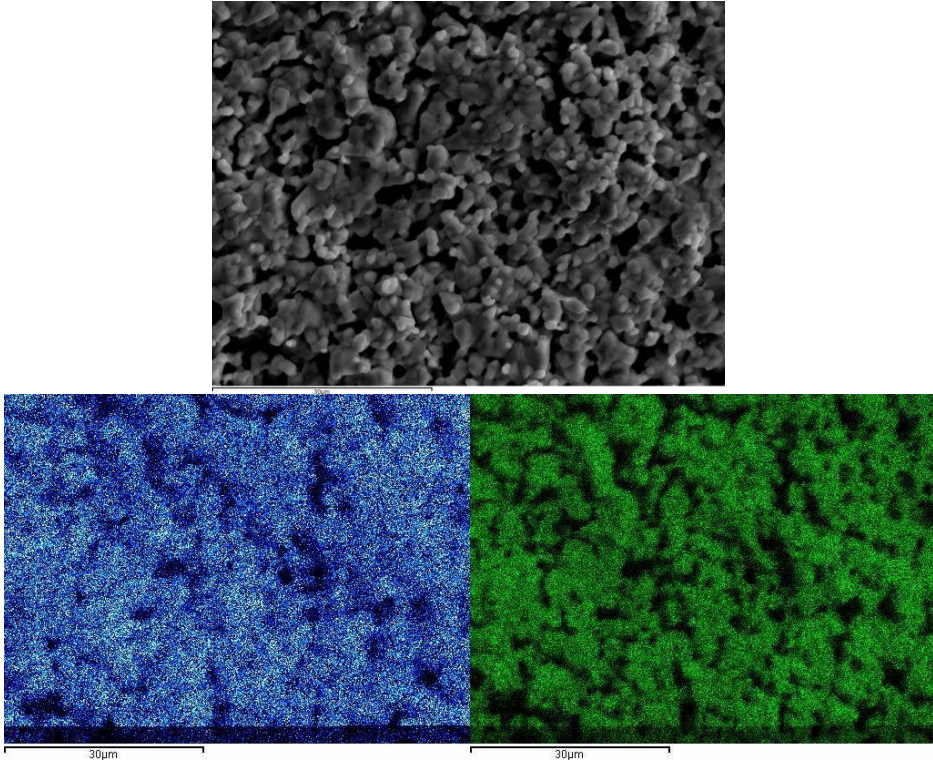

Figure 24: Mapping for the BTZ25 pellet with 4 thermal treatments.
The Zr mapping is shown in blue, the Ti mapping in green

3.5 ELECTRICAL CHARACTERIZATION

The densest pellet of BTZ25 was covered with a thin film of gold through a sputtering PVD. This film acts as a pair of electrodes. Once the borders of the pellet have been sanded down, when a voltage is applied to the system it becomes a capacitor.

The permittivity measurements were done from 50 K to 400 K, in order to observe the phase transition of the material. On the other hand, the sample's permittivity was measured at different

frequencies throughout this range of temperatures, with the aim of finding out the different contributions to the dielectric constant. The frequencies ranged from 200 Hz to 1 MHz.

In Figure 25 the two contributions to the complex permittivity are showed. The phase transition is clearly seen at 270 K, when the real contribution to permittivity (i.e. the dielectric constant) reaches its maximum. Therefore, the studied material is paraelectric at temperatures above this point, and becomes ferroelectric at lower temperatures. As it was expected, increasing the frequency of the AC makes the highest value of   decrease, because fewer mechanisms for polarization are allowed. On the opposite, dielectric losses increase with increasing frequency.
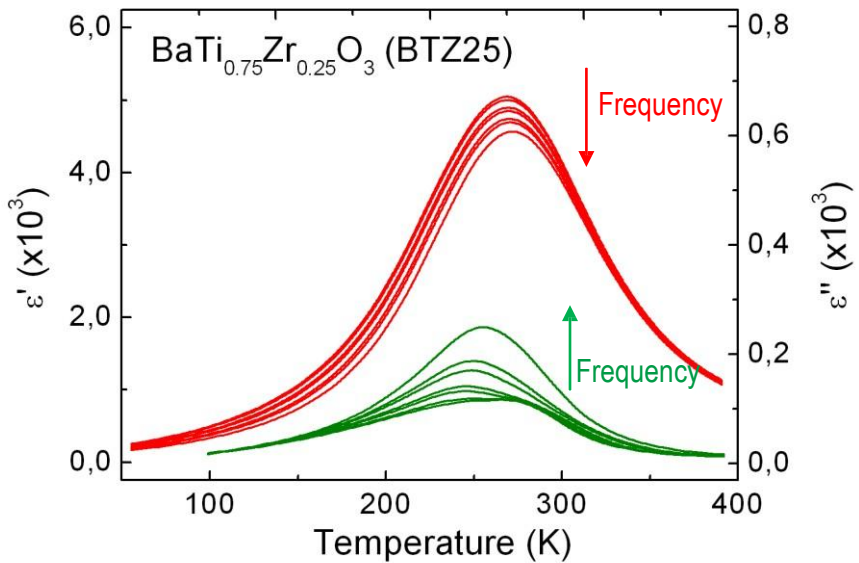

Figure 25: Dielectric response plot for a BTZ25 pellet. The green curves are referred to the right axis (dielectric looses) while the red curves are referred to the left axis (dielectric constant).

The loss tangent of a sample can be calculated to compare the results with previous works[12]. This magnitude is defined as:

$$\tan \delta = \frac{\varepsilon_r''}{\varepsilon_r'} x\ 100$$

The value is calculated at room temperature, for different frequencies. The results are shown in Table 2.

Entry	Frequency (kHz)		Entry	Frequency (kHz)	
1	0.2	1.26	11	20	1.67
2	0.3	1.29	12	30	1.70
3	0.5	1.32	13	50	1.76
4	0.7	1.34	14	70	1.84
5	1	1.39	15	100	1.87
6	2	1.45	16	200	2.03
7	3	1.50	17	300	2.17
8	5	1.53	18	500	2.43
9	7	1.56	19	700	2.69
10	10	1.59	20	1000	9.04

Table 2: Loss tangent for the compound BTZ25 at room temperature.

The values for dielectric constant in the studied sample range from 5000 to 4200 in its highest point. These values are lower than the reported in previous works, what can be justified by the low density of the pellet characterized. However, the loss tangent in the studied sample (1-2%) is slightly lower than the one found in the bibliography (2-4%). The only exception in this trend is in our measurement at 1MHz (entry 20), which gives an unusually high value for the loss tangent of 9%. This may mean that this measure is not reliable.

CONCLUSIONS:

After this essay had been completed, the following conclusions have been extracted:

- Electrical properties of solids depend of their composition and internal structure: space group, defects and grain boundaries.

- The ceramic method is a simple but very slow method for producing solid solutions. When increasing the proportion of zirconium in the material, the process needs an increase of the temperature or the time of the thermal treatment, because the greater radius of the Zr^{4+} ion makes the diffusion process more difficult.

- Grinding is vital to allow the homogeneity of the final material: if no grinding is carried out, diffusion through grain boundaries is not allowed and a multiple phased product is obtained, unless an extremely large thermal treatment is done.

- The high amount of energy necessary to maintain the pellets at 1500 ºC time enough for the diffusion to occur makes this method expensive. However, this is partly compensated by the price of the reactants, wich is cheaper than the ones used in other solid synthesis methods such as sol-gel (where metallic acetates or alcoxides are needed).

- Thermal analysis is a useful technique for the study of solid state reaction, since all the processes can be observed. Nevertheless, it can be difficult to assign the peaks to the processes.

- X-ray diffraction is a vital tool for material synthesis and characterization: it is a non-destructive test that shows whether there is a single-phased product or not by direct observation. Then, once a single phase is obtained, it allows the determination of the crystalline structure of our product.

- The morphology of materials can be studied by SEM. Coupled with an EDS analyzer this technique turns exceptionally powerful, for it gives a possibility to test

the homogeneity of the material in single phased products, and relate morphology and composition for multiple phased products. Due to this technique a hypothesis can be established: zirconium will lead to bigger grains than titanium in the solid solution BTZ, since the zirconium-rich areas in the BTZ35 pellet showed bigger grains than the titanium-rich ones. However, more studies should be done to confirm that hypothesis.

- Barium titanozirconate presents a good dielectric response, as it was expected from early works on this material.

Aknowledgements:

REFERENCES AND NOTES

(1) Cahn, R.W. *The coming of Material Sciences; Pergamon Materials Series*; Pergamon: Vol. Volume 5, pp 253-304.

(2) Cheetham, A.K. Advanced inorganic materials: An open horizon. *Science* **1994***, 264*, 794-795.

(3) Nanni, P.; Viviani, M.; Buscaglia, V. *Handbook of Low and High Dielectric Constant Materials and Their Applications* In *Chapter 9 - Synthesis of Dielectric Ceramic Materials;* Academic Press: Burlington, 1999; pp 429-455.

(4) Zhang, S.; Li, F. High performance ferroelectric relaxor-$PbTiO_3$ single crystals: Status and perspective. *J. Appl. Phys.* **2012***, 111*, 031301.

(5) West, A. R. *Solid state chemistry and its applications.* John Wiley & Sons: 1984 .

(6) Waser, R.; Bottger, U.; Tiedke, S. *Polar Oxides: Properties, Characterization, and Imaging;* John Wiley & Sons: 2006.

(7) Uchino, K. In *Handbook of Advanced Ceramics, Chapter 4 - 4.1 Piezoelectric Ceramics;* Academic Press: Oxford, 2003; pp 107-159.

(8) Kuang, S. J.; Tang, X. G.; Li, L. Y.; Jiang, Y. P.; Liu, Q. X. Influence of Zr dopant on the dielectric properties and Curie temperatures of $BaZr_xTi_{1-x}O_3$ ($0 \le x \le 0.12$) ceramics. *Scr. Mater.* **2009***, 61*, 68-71.

(9) EU-Directive 2002/96/EC: Waste electrical and electronic equipment (WEEE) . *Off. J. Eur. Union,* **2003**, 46, (L37),24-38.

(10) EU-Directive 2002/95/EC: Restriction of the use of certain hazardous substances in electrical and electronic equipment (RoHS). *Off. J. Eur. Union*, **2003**, *46* (L37), 19-23.

(11) Thakur, O. P.; Prakash, C.; James, A. R. Enhanced dielectric properties in modified barium titanate ceramics through improved processing. *J. Alloys Compounds* **2009***, 470*, 548-551.

(12) Tang, X.; Chew, K.; Chan, H. Diffuse phase transition and dielectric tunability of $BaZr_yTi_{1-y}O_3$ relaxor ferroelectric ceramics . *Acta Mater.* **2004***, 52*, 5177-5183.

(13) Moura, F.; Simoes, A. Z.; Stojanovic, B. D.; Zaghete, M. A.; Longo, E.; Varela, J. A. Dielectric and ferroelectric characteristics of barium zirconate titanate ceramics prepared from mixed oxide method. *J. Alloys Compounds* **2008***, 462*, 129-134.

(14) Guan, X.; Deng, X.; Lu, C.; Tan, Z.; Zhang, Y.; Yang, R.; Han, L. Structure and Dielectric Tunability of $BaTi_{1-y}Zr_yO_3$ Ferroelectric Ceramics. *Manufacturing Processes and Systems,* **2011***, 148-149*, 1091-1095.

(15) Julphunthong, P.; Bongkarn, T. Phase formation, microstructure and dielectric properties of $Ba(Zr_{0.1}Ti_{0.9}O_3$ ceramics prepared via the combustion technique. *Curr. Appl. Phys.* **2011***, 11*, S60-S65.

(16) Nakamoto, K. *Infrared spectra of inorganic and coordination compounds;* John Wiley &Sons: 1970.

(17) Last, J. T. Infrared-Absorption Studies on Barium Titanate and Related Materials. *Phys.Rev.* **1957***, 105*, 1740-1750.

(18) Sands, D. E. *Introducción a la cristalografía;* Reverté: 1993.

(19) Orazem, M. E.; Tribollet, B. An integrated approach to electrochemical impedance spectroscopy. *Electrochim. Acta* **2008***, 53*, 7360-7366.

(20) Strobel, R.; Maciejewski, M.; Pratsinis, S. E.; Baiker, A. Unprecedented formation of metastable monoclinic $BaCO_3$ nanoparticles. *Thermochimica Acta* **2006***, 445*, 23-26.

(21) Štefanić, G.; Popović, S.; Musić, S. The effect of mechanical treatment of zirconium(IV) hydroxide on its thermal behaviour. *Thermochimica Acta* **1995***, 259*, 225-234.

(22) Švadlák, D.; Shánělová, J.; Málek, J.; Pérez-Maqueda, L. A.; Criado, J. M.; Mitsuhashi, T. Nanocrystallization of anatase in amorphous TiO_2. *Thermochimica Acta* **2004***, 414*, 137-143.

(23) Rodriguez-Carvajal, J. AFFMA. Calcul des distances reticulaires avec tri affinement des parameters de maille. **1995**.